ACS NANO

www.acsnano.org

ARTICLE

Measuring the Ultrafast Spectral Diffusion and Vibronic Coupling Dynamics in CdSe Colloidal Quantum Wells using Two-Dimensional Electronic Spectroscopy

Hoang Long Nguyen, Thanh Nhut Do, Emek G. Durmusoglu, Merve Izmir, Ritabrata Sarkar, Sougata Pal, Oleg V. Prezhdo, Hilmi Volkan Demir,* and Howe-Siang Tan*

Cite This: https://doi.org/10.1021/acsnano.2c09606

Read Online

ACCESS | Metrics & More | Article Recommendations | Supporting Information

ABSTRACT: We measure the ultrafast spectral diffusion, vibronic dynamics, and energy relaxation of a CdSe colloidal quantum wells (CQWs) system at room temperature using two-dimensional electronic spectroscopy (2DES). The energy relaxation of light-hole (LH) excitons and hot carriers to heavy-hole (HH) excitons is resolved with a time scale of ∼210 fs. We observe the equilibration dynamics between the spectroscopically accessible HH excitonic state and a dark state with a time scale of ∼160 fs. We use the center line slope analysis to quantify the spectral diffusion dynamics in HH excitons, which contains an apparent sub-200 fs decay together with oscillatory features resolved at 4 and 25 meV. These observations can be explained by the coupling to various lattice phonon modes. We further perform quantum calculations that can replicate and explain the observed dynamics. The 4 meV mode is observed to be in the near-critically damped regime and may be mediating the transition between the bright and dark HH excitons. These findings show that 2DES can provide a comprehensive and detailed characterization of the ultrafast spectral properties in CQWs and similar nanomaterials.

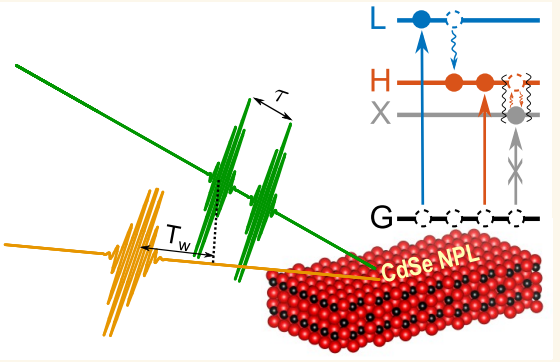

KEYWORDS: *two-dimensional electronic spectroscopy, spectral diffusion, colloidal quantum well, exciton, energy transfer, vibronic coupling*

Colloidal quantum wells (CQWs), also known as nanoplatelets (NPLs), are atomically flat quasi two-dimensional semiconductor nanocrystals. The ability to precisely control the shape, size, and composition of CQWs enables modification and control of their electronic and optical properties, which is important for various technological applications.[1−3] In the past decade, the synthesis process of colloidal cadmium selenide (CdSe) NPLs has been successfully developed with controllable thickness at atomic accuracy.[4,5] Each monolayer (ML) in CdSe NPLs consists of one Cd and one Se atomic layer and has a thickness of around 0.3 nm, thus making the thickness of several-ML NPLs much smaller than their lateral dimensions, which are usually tens to hundreds of nanometer. Due to the weak quantum confinement regime in the lateral dimensions, the position of the absorption edge, or the band gap, is mainly determined by the vertical thicknesses (z-direction) of the NPLs.[6] Upon excitation, the photogenerated electrons and holes also form excitons due to Coulombic interactions and are confined along the z-direction. The confinement along the z-direction can significantly increase the excitonic binding energy and red shift the excitonic absorption from the band edge.[7]

CdSe NPLs exhibit two sharp and strong excitonic absorption features, originating from the excitation of heavy-hole (HH) and light-hole (LH) excitons.[4,8] This is due to the quasi-2D geometry of NPLs, which confines the excitons in the vertical direction, causing the valence band to split into two bands with different effective masses (hence the name heavy- and light-hole band). In contrast, in the 3D-confined structure of the more well-studied quantum dots (QDs), there is no anisotropy. Subsequently, the hole states are degenerate, and

Received: September 27, 2022
Accepted: January 23, 2023

thus, the split into light and heavy hole is not found.[5,9,10] In NPLs, the LH excitons can quickly relax to HH at a time scale of 210 fs.[11] The HH excitons are further split into dark and bright states due to electron−hole exchange interactions,[12] with the bright state being predicted to be 3−4 meV higher in energy for 5-ML NPLs.[13] Although optically forbidden, the dark state can be populated through population transfer from the bright state. From fluorescence line narrowing and temperature-dependent photoluminescence (PL) experiments, the bright-dark equilibration time scale was determined to be ∼10−40 ps at 4 K,[13,14] while the time scale at room temperature has not yet been resolved. The recombination rates of bright and dark excitons were determined to be much slower, in the order of several nanoseconds, *via* PL and transient absorption (TA) measurements.[10,13−16]

NPLs offer several advantages compared to QDs for the investigation of their ultrafast properties. Thanks to their atomically precise synthesis and confinement only in the vertical dimension, NPL syntheses commonly yield magic-sized nanoparticles with the exact targeted number of monolayers featuring spectrally precise emission and absorption excitonic peaks and spectra, which is difficult to obtain to the same level of precision for the majority of the QD syntheses due to their typically wider size distribution and resulting size-dependent optical properties.[4,5] NPLs also possess additional useful features including a large exciton binding energy and giant oscillator strength, suitable for applications in optical gain, sensing, and photocatalysis.[1,5,17−21] Specifically, the applications in a variety of optoelectronic devices benefit from several advantages of NPLs over QDs. For example, the absorption cross-section of NPLs is very large, thanks to their tight vertical confinement and huge lateral dimensions.[19] The well-controlled vertical thickness and addition of heterostructures such as core/shell and core/crown[22−24] also allow for continuous tuning of the optical properties and charge carrier dynamics of the NPLs, making them a highly favorable group of precisely engineerable light-emitting materials.[2,25−27]

The various optoelectronic applications of nanomaterials require an in-depth understanding and characterization of its electronic properties and exciton dynamics, which are intimately influenced by the complex interactions between many electronic, vibronic, and other degrees of freedom. Time resolved TA spectroscopic techniques are the main tools to study such ultrafast dynamics. Two-dimensional electronic spectroscopy (2DES) adds on to the TA techniques in its ability to correlate detected signals to their corresponding excitation frequencies,[28] thus allowing us to identify complex processes that may be hidden in conventional TA spectroscopy. Such applications on the related nanostructure of CdSe QDs provide ample examples of the capabilities of these ultrafast techniques. TA has been performed on CdSe QDs to better resolve the spectral features and dynamics of energy states.[29−33] Recent 2DES studies on CdSe QDs have also provided information on their spectral line width broadening and spectral diffusion dynamics,[34,35] electronic coherences and dephasing mechanisms,[35,36] and multiexcitonic dynamics.[37]

In this study, we utilize 2DES to provide a comprehensive picture of the ultrafast dynamics taking place in colloidal CdSe NPLs upon being excited simultaneously at the HH and LH excitonic transitions. Recent TA measurements on CdSe NPLs studied the hole trapping dynamics and mechanisms.[38,39] There are several studies over the years focusing on the sub-picosecond dynamics of colloidal CdSe NPLs utilizing 2DES, with the main interests on the dynamics of heterostructures and electronic coherence.[11,38−40] Of considerable interest are the 2DES works by Cassette *et al.*, where electronic coherences of up to ∼100 fs were observed.[11,40] The study does not cover lower frequency coherences from other sources, such as vibronic coupling, that persist beyond the experimental time of these earlier experiments. There are many other unclarified properties in CdSe NPLs that 2DES is capable of characterizing and providing a more detailed analysis.

Excitonic coupling and energy transfers are the typical processes that can be directly observed in 2DES, as has been applied to several previous studies on various complex systems.[28,36,41−46] In addition, one phenomenon that can be measured in 2DES but is inaccessible using conventional TA spectroscopy is ultrafast spectral diffusion, which dictates the evolution of the 2D peakshapes due to the ability of 2DES to correlate the excitation and detection frequencies.[28] In ultrafast spectral diffusion, the excited system fluctuates and evolves to different frequencies in the time scale of femtoseconds to picoseconds due to interactions of the system with the environment, including coupling to vibrations of the proteins and/or solvent molecules in the environment as well as lattice phonon modes.[47−50] These ultrafast spectral diffusions take place at a much shorter time scale of the spectral diffusion measured by single-molecule PL studies on nanocrystals, which are at time scales of milliseconds to seconds.[51−54] One measure of the ultrafast spectral diffusion dynamics of an ensemble is the frequency-fluctuation correlation function (FFCF).[47,49,55] FFCF is a useful quantity as it connects microscopic molecular and atomic level dynamics directly to the nonlinear optical spectroscopic measurements such as 2DES. This can be based on a theoretical framework relying on diagrammatic time-dependent perturbation theory, Kubo line shape theory, and Brownian oscillator model.[28,47] Conversely, measuring the ultrafast spectral diffusion dynamics and FFCF provide insights into these couplings at the atomic and molecular level[48] and allow us to formulate appropriate mechanisms for understanding and optimizing various properties important in such CdSe NPL systems.

In this work, we measure the excitonic energy transfer dynamics between the LH and HH excitonic transitions, as well as the transfer dynamics between dark and bright states of the HH excitons. This is then followed by the measurement of the spectral diffusion dynamics and FFCF of the HH excitons. The subsequent analysis allows us to uncover the nature and strength of the vibronic coupling of the exciton to the various lattice phonon modes. This also sheds light on the possible mechanism of the measured transfer dynamics between the dark and bright states of the HH excitons. We show that 2DES is an excellent tool for studying optical properties of quantum systems such as NPLs, providing a single snapshot over the many possible transitions and deliver a comprehensive picture about the complicated dynamics in such quantum systems.

RESULTS AND DISCUSSION

Figure 1a illustrates the linear absorption spectrum of 5-ML CdSe NPLs and the excitation pulse spectrum used in the 2DES measurements. The two near-band-edge absorption peaks of CdSe NPLs center at 2.25 and 2.38 eV, corresponding to the absorption of HH and LH excitons, respectively. Spectral decomposition can be performed on the linear absorption spectrum to yield three components, as shown in

https://doi.org/10.1021/acsnano.2c09606
ACS Nano XXXX, XXX, XXX−XXX

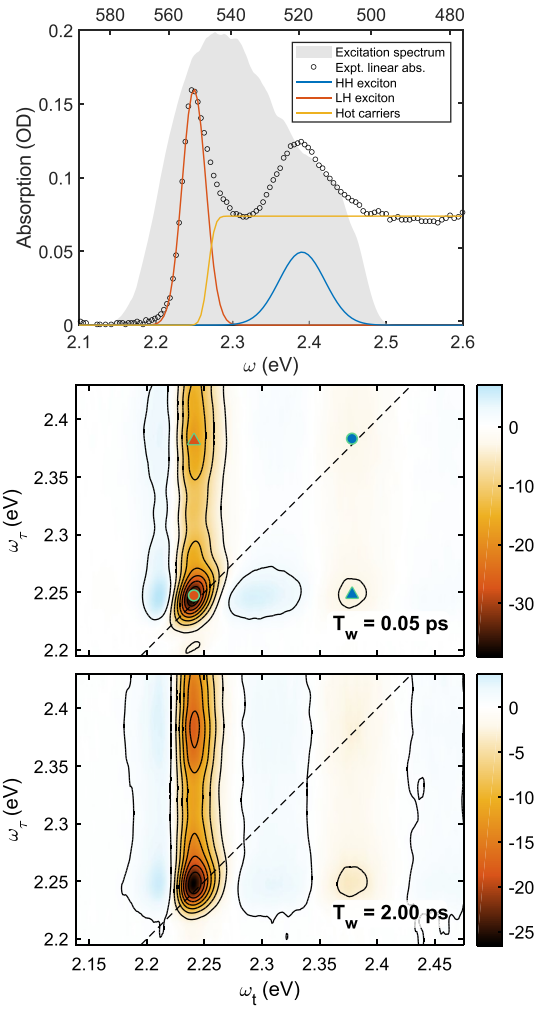

Figure 1. (a) Linear absorption of 5-ML CdSe NPLs (circles) with the fitted constituent components and the global fit (solid curves). The shaded area illustrates the excitation pulse spectrum used in the 2DES measurements. (b and c) Representative 2D spectra of 5-ML CdSe NPLs at the denoted waiting time T_w. The vertical and horizontal axes indicate the excitation and detection frequencies, respectively. The red and blue circles in the 2D spectra denote the centers of the diagonal peaks at (ω_τ, ω_t) = (2.25, 2.25) and (2.38, 2.38) eV, respectively. The red and blue triangles denote the centers of the crosspeaks at (ω_τ, ω_t) = (2.38, 2.25) and (2.25, 2.38) eV, respectively.

the figure, including two distinct Gaussian absorption peaks of the HH and LH excitons and an error function representing the absorption of hot carriers, *i.e.*, unbound electrons and holes.[56] The lateral size distributions of the synthesized NPLs can be determined from transmission electron micrographs (see the Supporting Information). In short, the lateral dimensions of the NPLs are about 32 ± 4 and 10 ± 2 nm and the area is about 309 ± 79 nm^2 (mean ± standard deviation).

Each 2D spectrum is an energy-correlation map between the vertical ω_τ and horizontal ω_t axis, representing the excitation and detection energies, respectively. Parts b and c of Figure 1 present the 2D spectra at waiting times T_w (time delays between the excitation and detection pulses) of 50 fs and 2 ps. In the 2DES experiment, a wide excitation spectrum was used to cover both the HH and LH excitonic transitions (see Figure 1a). The excitation fluence was low enough to avoid excessive excitation of hot carriers and multiexcitonic effects. The positions of the signals will be addressed using, respectively, the vertical and horizontal coordinates in the 2D map, (ω_τ, ω_t).

The main signals in the 2D spectra in Figure 1b,c concentrate around the HH and LH absorption regions. There are two negative diagonal peaks at (2.25, 2.25) and (2.38, 2.38) eV, respectively, for HH and LH excitons, and two negative off-diagonal peaks, or crosspeaks, at (2.25, 2.38) and (2.38, 2.25) eV, as shown in Figure 1b,c. The diagonal peaks are marked with circles, and the crosspeaks are marked with triangles. Negative signals on the diagonal are the results of the reduction in absorbance of the NPLs after the initial photoexcitation. Reduction in absorbance is usually due to the decrease in the ground-state (GS) population (or ground-state bleach, GB) and the increase in stimulated emission (SE) in the excited NPLs. An excitonic transition can also induce GB at another transition energy due to their shared GSs, resulting in crosspeaks. At later waiting times, the diagonal and crosspeak intensities may change due to population transfer and relaxation processes. In the case of NPLs, the shared electron states in the conduction band (CB) of HH and LH excitons result in negative crosspeaks appearing at very early waiting times, for example, in Figure 1b at T_w = 50 fs. In addition, the crosspeak at (2.38, 2.25) eV can have a contribution from the LH → HH relaxation.

Several positive signals, detected mainly at ω_t = 2.21 eV, and with smaller intensities at ω_t = 2.32 and 2.45 eV, can also be observed in Figure 1b,c. These positive features are photo-induced absorptions (PA), which are absorptions arising in the presence of the excited population. In this case, the PA signals can be seen as the additional absorption features appearing after the HH or LH excitons are created in the NPLs. Apart from the excitons, hot carriers are also created. However, the signals from hot carriers are barely detectable in the 2D spectra since most of them quickly relax to the band edge at low pump fluence.[57−59] In general, the spectral features in the 2D spectra are conserved during the observed T_w window from 50 fs to 2 ps, except for some minor changes in peakshapes and peak intensities. These changes reflect various ultrafast processes happening in CdSe CQWs.

In the high excitation energy region (ω_τ = 2.30−2.45 eV), the excited species include the LH excitons and hot carriers, with the possible detected signals depicted in Figure 2a. These states, upon excitation, quickly relax to the HH excitonic states.[11] To quantify this process, we integrate over the area containing these species' signals and plot them as a function of the waiting time T_w (Figure 2b). The resultant kinetic traces allow us to further analyze the population kinetics. Along the excitation axis ω_τ, the integrated areas span from 2.34 to 2.43 eV. Along the detection axis ω_t, the blue area covers the signals from 2.26 to 2.43 eV, which tracks the total signals from LH excitons and hot carriers. Meanwhile, the red area integrates the signals from ω_t = 2.19 to 2.24 eV, containing the signals of HH excitons. These areas are illustrated in the inset of Figure 2b. The integrated signals of these areas, *i.e.*, the kinetic traces, can be fitted with single-exponential functions, which give similar lifetimes of ∼210 fs (Table 1). In TA and 2D spectroscopy, concomitant rise and decay of sets of peaks at similar time scales typically indicate a population transfer process.[41,60] The kinetic traces in Figure 2b thus represent the hole transfer process where the hole population initially excited

https://doi.org/10.1021/acsnano.2c09606
ACS Nano XXXX, XXX, XXX−XXX

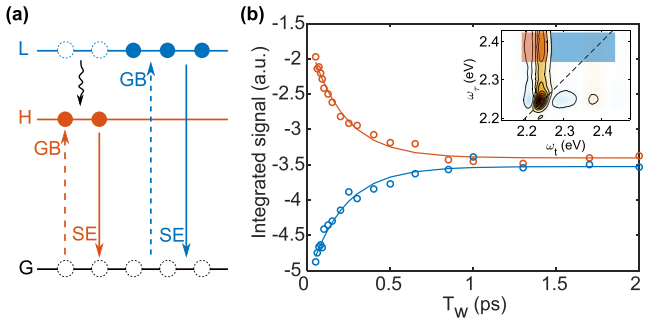

Figure 2. (a) 2D signals observed after initial excitation of the NPLs at the LH excitonic transition. Presenting in an excitonic representation, G, H, and L represent the ground state (GS), HH, and LH excitonic states, respectively. The excitons are initially excited to L state and then partly relaxed to H state. The dotted circles represent populations before being excited or relaxed. The probe pulse detects lesser absorption (GB, dashed arrows) and more emission (SE, solid arrows) in both L and H states, resulting in negative transient absorption signals. PA processes are not shown. (b) Integrated signals (circles) of the spectral regions where LH excitons and hot carriers are excited, along with the exponential fits (solid curves). The blue curve represents the combined population of the LH excitons and hot carriers, while the red curve represents the HH excitons population. The corresponding integrated areas on the 2D spectrum are shaded in the inset.

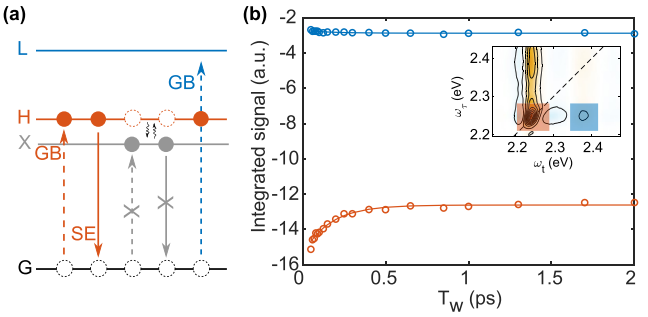

Figure 3. (a) 2D signals recorded initial excitation of the NPLs at the HH excitonic transition. X represents a spectroscopically inaccessible (dark) state. The excitons are initially excited to H state and then partly equilibrate with X state. (b) Integrated signals (circles) of the spectral regions where HH excitons are excited, along with the exponential fits (solid curves). Red represents the HH exciton population, while blue tracks the GB signals at LH excitonic transition. The corresponding integrated regions on the 2D spectrum are shaded in the inset.

Table 1. Fitting Parameters of the Kinetic Traces Presented in Figures 2 and 3[a]

signal at (ω_τ, ω_t)	a (a.u.)	T (ps)	a_0 (a.u.)
(2.34−2.43,2.26−2.43) eV—Figure 2b, blue area	−1.62	0.21	−3.53
(2.34−2.43,2.19−2.24) eV—Figure 2b, red area	+1.73	0.21	−3.40
(2.21−2.28,2.35−2.42) eV—Figure 3b, blue area	+0.17	0.17	−2.88
(2.21−2.28,2.21−2.28) eV—Figure 3b, red area	−2.81	0.16	−12.62

[a]All are fitted with exponential functions $f(T_w) = ae^{-T_w/T} + a_0$.

at the LH−CB energy gap transfers to the HH band. A similar observation was also made by Cassette *et al.*[11]

In the low excitation energy region (ω_τ = 2.2−2.3 eV), the diagonal peak at (2.25, 2.25) eV represents the GB and SE signals of the HH excitonic transition. The kinetics of this peak is plotted in Figure 3b with the integrated signal of the area around the diagonal. The kinetics can be fitted with a single-exponential decay with a time scale of ∼160 fs (Table 1). The kinetic decreases by 2.81 in amplitude to a baseline of −12.6, a decrease of ∼22%, and is attributed to the reduction of the GB and SE signal contribution. The crosspeak at (2.25, 2.38) eV (blue curve in Figure 3b) represents the LH GB signal upon HH excitation, due to their shared electron states. From Table 1, the crosspeak signal increases by 0.17 in amplitude out of a baseline of −2.88 (∼6%), which is much lesser than the decrease of the diagonal peak. Thus, apart from the decay in amplitude of the negative diagonal peak, there is no concomitant rise observed in the 2D spectra. The absence of a significant rising signal at ∼160 fs suggests that the population transfer from HH is to a state X that is spectroscopically inaccessible, which can be referred to as a dark state. The identity of state X will be discussed later. Previously, Cassette *et al.* observed a similar decay in the HH exciton signal using TA spectroscopy and assigned it to a generic hole-trapping process.[40] Figure 3a provides a schematic to summarize the associated dynamics of the HH and LH excitons and the dark state X after excitation at the HH transition.

Apart from the dynamical changes in amplitude, another main observation is the time evolution of the shape of the 2.25 eV diagonal peak. The time evolution of the peakshape contains information on the homogeneity, inhomogeneity, and ultrafast spectral diffusion dynamics of the transition. During spectral diffusion, fluctuation in the transition frequency causes the correlation between the excitation and emission energy to decrease.[28,49] This trend manifests itself in the 2D spectra peakshape, changing from an elongated peak along the diagonal to a broader, more vertically aligned peak with increasing waiting time T_w.[49] This can be seen in Figure 4a, which depicts the 2.25 eV diagonal peak at two T_ws. At T_w = 50 fs, the peak is elongated, and its tilt is aligned toward the diagonal. By T_w = 2 ps, the peak becomes more spherical due to spectral diffusion. One can also intuitively see this broadening effect due to spectral diffusion by taking a spectral slice at ω_τ = 2.25 eV from the 2D spectra at T_w = 0.05 and 2 ps. The comparison between the two spectral lineshapes (as a function of ω_t) is wider for the T_w = 2 ps spectrum. Details of this T_w dependent broadening trend are provided in the Supporting Information (Figure S3). As mentioned in the introduction, FFCF provides a meaningful expression for such spectral diffusion. One way to characterize the spectral diffusion process and FFCF is to measure the tilt of the 2.25 eV diagonal peak in a process known as center line slope (CLS) analysis. The detailed procedure of CLS extraction is provided elsewhere.[49] In our study, the CLS is obtained from the line, as indicated by the white dots and green overlay fit lines of the 2D peakshape in Figure 4a. The slope of this line is taken with respect to the vertical axis (ω_τ-axis), and the resulting CLS values are reported in Figure 4b. Importantly, the CLS value gives a direct measurement of the normalized FFCF.[49,50,61] The FFCF quantifies the exciton's fluctuation and coherent dynamical change in its transition energy, due to various intra- and intermolecular processes.[28] In general, a higher slope (high CLS value) corresponds to a higher degree of correlation between ω_τ and ω_t; thus, a spectral diffusion

https://doi.org/10.1021/acsnano.2c09606
ACS Nano XXXX, XXX, XXX−XXX

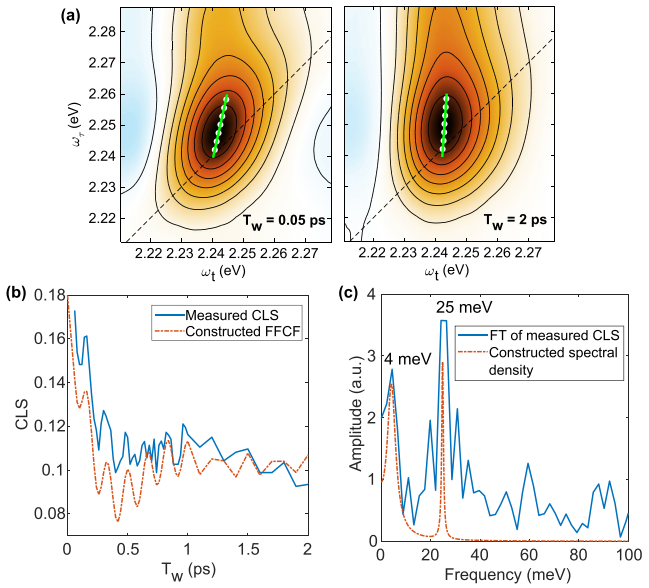

Figure 4. (a) Examples of the center lines of the 2.25 eV diagonal peak, from which the slope with respect to the vertical axis is obtained as the CLS. The measured CLS plot with waiting time T_w and its Fourier transform are shown in blue color in (b) and (c), respectively. The T_w step in the CLS plot is 25 fs, and after 1 ps, it becomes 100 fs. The Fourier transform is performed on the first 1 ps. A constructed spectral density $C(\omega)$ with two modes, whose parameters are listed in Table 2, and the CLS plot constructed from it are also shown in red color in (c) and (b), respectively.

process results in a decaying CLS. Furthermore, coherent dynamics such as those due to vibronic coupling can also cause oscillations in the CLS measurements.[50,62]

The CLS analysis results for the 2.25 eV diagonal peak are shown in Figure 4b. At 50 fs, the shortest T_w of our data, the CLS has a value of ∼0.18. The CLS then appears to decay at a few-hundred-femtosecond time scale while exhibiting clear oscillatory features. At longer T_ws, the CLS settles to a value of ∼0.1. As the CLS recovers the normalized FFCF, the theoretical CLS value at T_w = 0 fs should be unity. Nevertheless, the measured CLS value has dropped to a value of only ∼0.18 at our first data point of T_w = 50 fs. This suggests that a large decay of the FFCF happens in the sub-50 fs time scale, which our experiment does not capture. In addition, in FFCFs, a constant baseline represents an inhomogeneous component.[49,61] We can therefore assign the constant value of CLS of ∼0.1 at a long T_w to the inhomogeneity of the NPLs ensemble.

We next analyze the oscillatory features, which can be characterized more clearly as a Fourier transform of the measured CLS (Figure 4c). The key features of the resultant Fourier transform map peak at 4 and 25 meV, which correspond to beating periods of ∼1 ps and ∼170 fs, respectively. The evolution of the CLS, *i.e.*, the FFCF, can be modeled using a well-established system-bath model, where the HH−CB transition is coupled to a bath of harmonic oscillators described by a spectral density function $C(\omega)$.[47,63] These couplings cause fluctuations in the system transitions and result in the observed spectral diffusion and beating dynamics.[47] Since the CLS measures the normalized FFCF, the resultant Fourier transform of the CLS can be viewed as proportional to the spectral density $C(\omega)$ of the bath, which couples to the HH−CB transition. We can model the spectral density $C(\omega)$ using a series of damped oscillators of energy ω_j, damping constant γ_j, and relative coupling strength λ_j. At the high-temperature limit, $C(\omega)$ can be expressed as (see the SI for detailed derivations):[63]

$$C(\omega) \sim \sum_j \frac{\lambda_j \omega_j \gamma_j (\omega^2 + \omega_j^2 + \gamma_j^2)}{(\omega^2 + \omega_j^2 + \gamma_j^2)^2 - 4\omega^2\omega_j^2} \quad (1)$$

To phenomenologically replicate the measured CLS, we construct a spectral density $C(\omega)$ using two modes (4 and 25 meV) with the parameters listed in Table 2 and portrayed in Figure 4c. The constructed FFCF is obtained by inverse Fourier transforming $C(\omega)$ and added a baseline of ∼0.1 to account for the inhomogeneous component and then compared to the measured CLS as depicted in Figure 4b. The main features of the measured CLS can be observed to be replicated quite well in the constructed FFCF, including the apparent sub-200 fs initial drop and oscillatory patterns with the correct phase dependence. In the parameters used, the 4 meV mode is in the near-critically damped regime, with $\omega_1 \approx \gamma_1$, where the oscillation only survives for about one cycle. The observation of the sub-200 fs drop from ∼0.18 to ∼0.1 on the experimental CLS (Figure 4b) can therefore be explained as part of this 4 meV near-critically damped oscillation. If we treat this drop as an exponential decay and attempt to fit it to the measured CLS at larger T_w steps (thus ignoring the higher frequency beatings), we obtain a decay of ∼160 fs (see the SI). The second mode used in the model with an energy of 25 meV is in the regime of underdamped mode, with $\omega_2 \gg \gamma_2$ and explains the 170 fs oscillations. The inverse of the damping constant γ_i gives the time scale of the decay of the oscillation signal and hence a measurement of the dephasing or decoherence time. This gives an approximate decoherence time for the 4 meV mode of ∼330 fs. This decoherence time may not be clearly discernible in the CLS plot in Figure 4b, as the falling edge of the first cycle of the 170 fs oscillation dominates the signal.

Table 2. Parameters for the Constructed Spectral Density in Figure 4c

mode j	energy, $\omega_j/2\pi$ (meV)	damping constant, $\gamma_j/2\pi$ (meV)	relative strength, λ_j (a.u.)
1	4	2	1
2	25	0.4	0.04

Quantum-mechanical calculations are performed on the 5-ML CdSe NPL structure to provide further insights to the analysis. The details of the calculations are summarized in the SI and can be found in previous publications.[64−66] In short, the NPLs in the simulation are capped with acetic acid and geometrically optimized at 0 K and then heated to 300 K and simulated with molecular dynamics (MD). MD snapshots are generated until 3 ps with 1 fs time steps. The electronic structures are obtained from density functional tight binding (DFTB) calculations. Figure 5a depicts the top and side views of the optimized NPL. The electronic transitions obtained from every MD snapshot are used to estimate the early time behavior of the autocorrelation function, or normalized FFCF, of the energy gap between the HH and GS. In Figure 5b, we show the calculated normalized FFCF for the two main HH transitions identified in the calculation, labeled as HX1 and HX2. As can be seen, the FFCF experiences a decay with a

https://doi.org/10.1021/acsnano.2c09606
ACS Nano XXXX, XXX, XXX−XXX

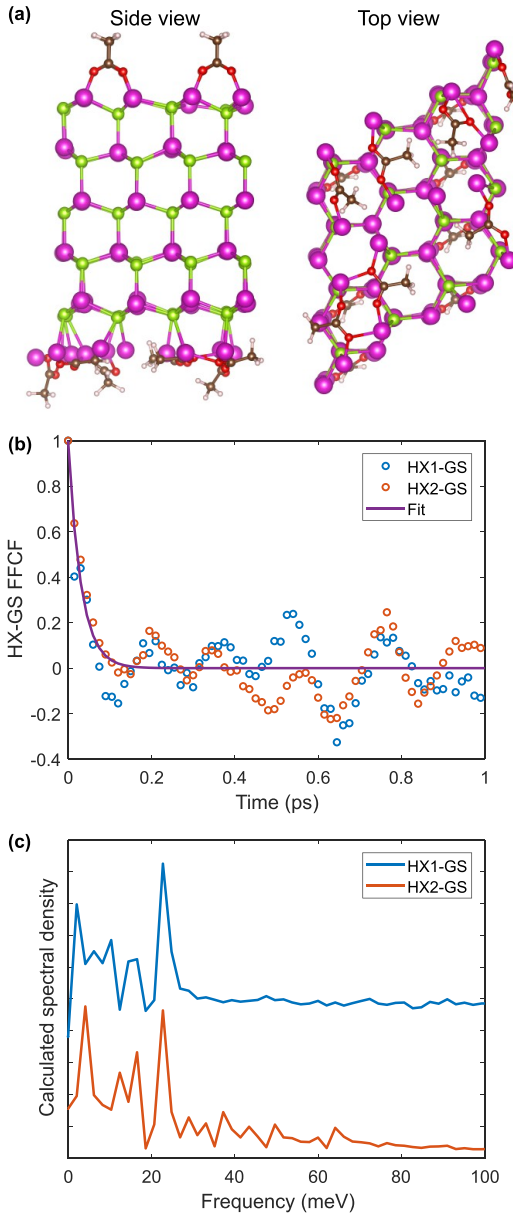

Figure 5. (a) Side and top views of the optimized 5-ML CdSe NPL structure, capped with acetic acid. The Cd, Se, O, C, and H atoms are denoted with purple, green, red, brown, and gray spheres, respectively. (b) Normalized FFCF of the energy gap HX1-GS (blue) and HX2-GS (red) transitions, obtained from the quantum-mechanical calculations. Both FFCFs are fitted simultaneously with a single-exponential function, yielding a lifetime of ∼30 fs. (c) Fourier transformations of the calculated HX-GS FFCFs, where the HX1-GS plot is translated vertically for clarity.

lifetime of ∼30 fs and exhibits oscillatory features. The spectral densities of the HX-GS transitions are shown in Figure 5c, obtained by taking the Fourier transformation of the corresponding calculated FFCF. The fast ∼30 fs decay arises from the initial dephasing of all the modes present in the spectral density, mainly ranging up to ∼25 meV. This can be assigned to the drop of the measured CLS value to ∼0.2 at T_w = 50 fs, which is too fast to be resolved in our experiment.

The calculated spectral densities also peak at ∼4 and ∼25 meV (Figure 5c). This is consistent with the modes obtained from the experimental CLS's oscillatory features (Figure 4c). The 4 meV peak corresponds to the acoustic phonon mode in the CdSe lattice.[67−70] The higher energy modes can be assigned to the surface acoustic (SA) phonon modes due to the out of lattice movement between Cd atoms and ligands at the NPLs surface.[70] They can also be due to the surface optical (SO) and longitudinal optical (LO) modes.[64,71] The reason behind the appearance of SO modes can be explained by the elongation and shortening of the bonds between surface Cd and ligands. In the calculations, the modes appear as underdamped. However, our experiments suggest that the 4 meV mode is nearer to the critically damped regime.

The identity of the spectroscopically inaccessible dark state X will now be discussed. One possible assignment of X is a dark excitonic state that is close in energy and in equilibration with the bright HH excitonic state, as suggested in several studies.[12−14,72] The bright-dark exciton splitting has been measured to be 3−4 meV for 5-ML CdSe NPLs.[13] Furthermore, the energy of the near-critically damped phonon mode of 4 meV observed in our CLS analysis thus matches the energy gap between the bright and dark exciton. It has been hypothesized that the transition between the bright and dark states requires a spin-flip with a corresponding emission or absorption of acoustic phonons.[14,73] Thus, it is likely that the bright-dark exciton equilibration is mediated by the 4-meV acoustic phonons in the CdSe lattice. We also note that the apparent decay (*i.e.*, the initial decrease of a near-critically damped oscillation) time scale of ∼160 fs is similar to the decay time scale of the integrated signal of the area around the HH diagonal peak at (2.25, 2.25) eV, which, as analyzed earlier, is due to the population transfer to a spectroscopically inaccessible state X. We conjecture that these two processes measured at ∼160 fs are associated with each other, and thus, the state X can be assigned as the dark state of the HH exciton. Conversely, the 25 meV mode is observed to be underdamped possibly because of the absence of decay channels between states of comparable energy gap in this system.

CONCLUSIONS

In conclusion, using 2DES as the main tool for observation of the dynamics of 5-ML CdSe NPLs, various processes taking place at sub-picosecond time scales can be observed. These include the energy relaxation from LH excitons and hot carriers to HH excitons, the energy flow of HH excitons to a dark state, spectral diffusion dynamics of the HH excitons, and their vibronic couplings to various phonon modes. The participation of the lattice phonon modes in the fluctuations of excitonic transitions can be well-reproduced in our quantum-mechanical calculations.

It is worth noting that 2DES was able to resolve various spectral features in both time and frequency domains. Thus, 2DES can provide extra information that may be crucial in identifying the participating species, such as characterizing the properties of the dark excitons in nanomaterials, which previously relied on observations at very low temperature.[13] The observation of the bright-dark equilibration using the associated spectral diffusion process, which can only be quantified using 2D spectra, is also an excellent example of the strength of 2DES. Further 2DES investigations of different heterostructures and hybrids of NPLs are expected to provide valuable insights about the gain mechanisms of CQWs, which is a very active research direction in the scientific community of colloidal nanocrystals.

https://doi.org/10.1021/acsnano.2c09606
ACS Nano XXXX, XXX, XXX−XXX

METHODS

Synthesis of 5-ML CdSe NPLs. 5-ML CdSe NPLs were prepared according to the reported procedure with slight modifications.[7] Cadmium myristate (340 mg) and 27 mL of ODE were loaded into a three-neck flask and degassed for 1 h at 95 °C under a vacuum. Subsequently, the reaction mixture temperature was raised to 250 °C under constant argon flow, and a solution of 3 mL of 0.15 M ODE-Se was quickly injected. Next, 160 mg of cadmium acetate dehydrate was added to initiate lateral growth. The solution was kept at 250 °C for 7 min. The reaction was then terminated with an injection of 1 mL of oleic acid and cooled to room temperature by using a water bath. The resulting CdSe NPLs were centrifuged to remove nonreacted precursors. Finally, the obtained solution was washed with acetone, and the cleaned NPLs were dispersed in hexane.

2DES Measurement. Ultrafast 2DES measurement was performed using the partially collinear pump−probe geometry. Laser pulses from a 1 kHz, 800 nm Ti:sapphire amplifier (Legend Elite, Coherent) were focused to a 2 m long tube containing 2.2 bar of pressurized argon. A continuum was generated by self-phase modulation[74,75] inside the tube and split using a UV-fused silica wedged window. The reflected beam from the wedged window was compressed by 10 reflection roundtrips on a pair of chirped mirrors (DMC9, Laser Quantum) and further split by a 50/50 beamsplitter to use as the probe and reference beams. The pump beam, transmitted part from the wedged window, was sent to a single-prism compressor[76] and shaped by an acousto-optic pulseshaper (Dazzler, Fastlite). The resulting pump pulse has an approximately 240 meV spectral full width at half-maximum (see Figure 1a) and is compressed to ∼25 fs as measured using an autocorrelator (pulseCheck). The pulse is approximately 3 times transform limited. The beam was shaped into a double-pulse train with controllable interpulse delay τ, ranging from 0 to 120 fs with 3 fs steps, and a phase relationship following 1 × 2 phase cycling scheme.[77] The power of the pump pulse was limited to 0.5 nJ per pulse so that the pump fluence was low enough to avoid the excitation of high-temperature carriers and multiexciton effects. The pump, probe, and reference beam were focused on the sample using an off-axis parabolic mirror. The waiting time T_w between the pump and probe pulse was controlled using a retroreflector mounted on a linear motorized stage (Physik Instrumente). The signal emitted from the sample was guided to a spectrometer, where it was spectrally dispersed to a CCD array (PIXIS, Princeton Instruments) and recorded along ω_t axis. A series of τ-dependent TA spectra, $\Delta A(\tau, T_w, \omega_t)$, were obtained at each T_w, which was then Fourier transformed along τ to generate a 2D spectrum $S^{2D}(\omega_\tau, T_w, \omega_t)$. The measurement was repeated twice with separately synthesized sample batches to ensure the reproducibility.

ASSOCIATED CONTENT

Supporting Information

The Supporting Information is available free of charge at https://pubs.acs.org/doi/10.1021/acsnano.2c09606.

Discussions of sample characterization, center line slope of HH diagonal peak, spectral broadening during spectral diffusion, derivation of the spectral density function, and quantum-mechanical calculations and figures of scatter plot, CLS plot of HH diagonal peak with single-exponential fit, and 2D spectra (PDF)

AUTHOR INFORMATION

Corresponding Authors

Hilmi Volkan Demir − *LUMINOUS! Centre of Excellence for Semiconductor Lighting and Displays, The Photonics Institute, School of Electrical and Electronic Engineering and School of Materials Science and Engineering, Nanyang Technological University, Singapore 639798, Singapore; Division of Physics and Applied Physics, School of Physical and Mathematical Sciences, Nanyang Technological University, Singapore 637371, Singapore; Department of Electrical and Electronics Engineering, Department of Physics, UNAM—Institute of Materials Science and Nanotechnology, Bilkent University, Ankara 06800, Turkey;* orcid.org/0000-0003-1793-112X; Email: volkan@stanfordalumni.org

Howe-Siang Tan − *School of Chemistry, Chemical Engineering and Biotechnology, Nanyang Technological University, Singapore 637371, Singapore;* orcid.org/0000-0003-2523-106X; Email: howesiang@ntu.edu.sg

Authors

Hoang Long Nguyen − *School of Chemistry, Chemical Engineering and Biotechnology, Nanyang Technological University, Singapore 637371, Singapore; University of Groningen, Zernike Institute for Advanced Materials, 9747 AG Groningen, The Netherlands*

Thanh Nhut Do − *School of Chemistry, Chemical Engineering and Biotechnology, Nanyang Technological University, Singapore 637371, Singapore;* Present Address: Department of Physics and Astronomy, Faculty of Science, Vrije Universiteit Amsterdam, De Boelelaan 1081, 1081 HV Amsterdam, The Netherlands; orcid.org/0000-0002-5155-6936

Emek G. Durmusoglu − *LUMINOUS! Centre of Excellence for Semiconductor Lighting and Displays, The Photonics Institute, School of Electrical and Electronic Engineering, Nanyang Technological University, Singapore 639798, Singapore; Division of Physics and Applied Physics, School of Physical and Mathematical Sciences, Nanyang Technological University, Singapore 637371, Singapore;* orcid.org/0000-0001-6840-8342

Merve Izmir − *LUMINOUS! Centre of Excellence for Semiconductor Lighting and Displays, The Photonics Institute, School of Electrical and Electronic Engineering and School of Materials Science and Engineering, Nanyang Technological University, Singapore 639798, Singapore*

Ritabrata Sarkar − *Department of Chemistry, University of Gour Banga, Malda 732103, India; Bremen Center for Computational Materials Science, University of Bremen, Bremen 28359, Germany;* orcid.org/0000-0001-7798-1140

Sougata Pal − *Department of Chemistry, University of Gour Banga, Malda 732103, India;* orcid.org/0000-0002-1514-2728

Oleg V. Prezhdo − *Department of Chemistry, University of Southern California, Los Angeles, California 90089, United States;* orcid.org/0000-0002-5140-7500

Complete contact information is available at: https://pubs.acs.org/10.1021/acsnano.2c09606

Notes

The authors declare no competing financial interest.

ACKNOWLEDGMENTS

H.V.D. gratefully acknowledges the financial support in part from the Singapore Agency for Science, Technology and Research (A*STAR) SERC under Grant No. M21J9b0085, and the Singapore Ministry of Education Tier 1 grant (MOE-RG62/20). H.V.D. also gratefully acknowledges the support from TUBA. H.-S.T. gratefully acknowledges the financial support in part from the Singapore Ministry of Education Tier

https://doi.org/10.1021/acsnano.2c09606
ACS Nano XXXX, XXX, XXX−XXX

1 grant (MOE-RG2/19 and MOE-RG14/20). O.V.P. acknowledges the financial support from the United States National Science Foundation under Grant No. CHE-2154367.

REFERENCES

(1) Yu, J.; Chen, R. Optical Properties and Applications of Two-Dimensional Cdse Nanoplatelets. *InfoMater.* **2020**, *2*, 905−927.
(2) She, C.; Fedin, I.; Dolzhnikov, D. S.; Dahlberg, P. D.; Engel, G. S.; Schaller, R. D.; Talapin, D. V. Red, Yellow, Green, and Blue Amplified Spontaneous Emission and Lasing Using Colloidal Cdse Nanoplatelets. *ACS Nano* **2015**, *9*, 9475−9485.
(3) Dutta, A.; Medda, A.; Patra, A. Recent Advances and Perspectives on Colloidal Semiconductor Nanoplatelets for Optoelectronic Applications. *J. Phys. Chem. C* **2021**, *125*, 20−30.
(4) Ithurria, S.; Dubertret, B. Quasi 2d Colloidal Cdse Platelets with Thicknesses Controlled at the Atomic Level. *J. Am. Chem. Soc.* **2008**, *130*, 16504−16505.
(5) Ithurria, S.; Tessier, M. D.; Mahler, B.; Lobo, R. P.; Dubertret, B.; Efros, A. L. Colloidal Nanoplatelets with Two-Dimensional Electronic Structure. *Nat. Mater.* **2011**, *10*, 936−941.
(6) Davies, J. H.*The Physics of Low-Dimensional Semiconductors: An Introduction*; Cambridge University Press: New York, 1998.
(7) Failla, M.; García Flórez, F.; Salzmann, B. B. V.; Vanmaekelbergh, D.; Stoof, H. T. C.; Siebbeles, L. D. A. Observation of the Quantized Motion of Excitons in Cdse Nanoplatelets. *Phys. Rev. B* **2020**, *102*, 195405.
(8) Yeltik, A.; Delikanli, S.; Olutas, M.; Kelestemur, Y.; Guzelturk, B.; Demir, H. V. Experimental Determination of the Absorption Cross-Section and Molar Extinction Coefficient of Colloidal Cdse Nanoplatelets. *J. Phys. Chem. C* **2015**, *119*, 26768−26775.
(9) Morgan, D. P.; Kelley, D. F. Exciton Localization and Radiative Lifetimes in Cdse Nanoplatelets. *J. Phys. Chem. C* **2019**, *123*, 18665−18675.
(10) Morgan, D. P.; Maddux, C. J. A.; Kelley, D. F. Transient Absorption Spectroscopy of Cdse Nanoplatelets. *J. Phys. Chem. C* **2018**, *122*, 23772−23779.
(11) Cassette, E.; Pensack, R. D.; Mahler, B.; Scholes, G. D. Room-Temperature Exciton Coherence and Dephasing in Two-Dimensional Nanostructures. *Nat. Commun.* **2015**, *6*, 6086.
(12) Efros, A. L.; Rosen, M.; Kuno, M.; Nirmal, M.; Norris, D. J.; Bawendi, M. Band-Edge Exciton in Quantum Dots of Semiconductors with a Degenerate Valence Band: Dark and Bright Exciton States. *Phys. Rev. B* **1996**, *54*, 4843−4856.
(13) Shornikova, E. V.; Biadala, L.; Yakovlev, D. R.; Sapega, V. F.; Kusrayev, Y. G.; Mitioglu, A. A.; Ballottin, M. V.; Christianen, P. C. M.; Belykh, V. V.; Kochiev, M. V.; et al. Addressing the Exciton Fine Structure in Colloidal Nanocrystals: The Case of Cdse Nanoplatelets. *Nanoscale.* **2018**, *10*, 646−656.
(14) Biadala, L.; Liu, F.; Tessier, M. D.; Yakovlev, D. R.; Dubertret, B.; Bayer, M. Recombination Dynamics of Band Edge Excitons in Quasi-Two-Dimensional Cdse Nanoplatelets. *Nano Lett.* **2014**, *14*, 1134−1139.
(15) Kunneman, L. T.; Schins, J. M.; Pedetti, S.; Heuclin, H.; Grozema, F. C.; Houtepen, A. J.; Dubertret, B.; Siebbeles, L. D. Nature and Decay Pathways of Photoexcited States in Cdse and Cdse/Cds Nanoplatelets. *Nano Lett.* **2014**, *14*, 7039−7045.
(16) Olutas, M.; Guzelturk, B.; Kelestemur, Y.; Yeltik, A.; Delikanli, S.; Demir, H. V. Lateral Size-Dependent Spontaneous and Stimulated Emission Properties in Colloidal Cdse Nanoplatelets. *ACS Nano* **2015**, *9*, 5041−5050.
(17) Altintas, Y.; Gungor, K.; Gao, Y.; Sak, M.; Quliyeva, U.; Bappi, G.; Mutlugun, E.; Sargent, E. H.; Demir, H. V. Giant Alloyed Hot Injection Shells Enable Ultralow Optical Gain Threshold in Colloidal Quantum Wells. *ACS Nano* **2019**, *13*, 10662−10670.
(18) Dede, D.; Taghipour, N.; Quliyeva, U.; Sak, M.; Kelestemur, Y.; Gungor, K.; Demir, H. V. Highly Stable Multicrown Heterostructures of Type-Ii Nanoplatelets for Ultralow Threshold Optical Gain. *Chem. Mater.* **2019**, *31*, 1818−1826.
(19) Pelton, M. Carrier Dynamics, Optical Gain, and Lasing with Colloidal Quantum Wells. *J. Phys. Chem. C* **2018**, *122*, 10659−10674.
(20) Sigle, D. O.; Zhang, L.; Ithurria, S.; Dubertret, B.; Baumberg, J. J. Ultrathin Cdse in Plasmonic Nanogaps for Enhanced Photocatalytic Water Splitting. *Journal of Physical Chemistry Letters.* **2015**, *6*, 1099−1103.
(21) Lorenzon, M.; Christodoulou, S.; Vaccaro, G.; Pedrini, J.; Meinardi, F.; Moreels, I.; Brovelli, S. Reversed Oxygen Sensing Using Colloidal Quantum Wells Towards Highly Emissive Photoresponsive Varnishes. *Nat. Commun.* **2015**, *6*, 6434.
(22) Rossinelli, A. A.; Riedinger, A.; Marqués-Gallego, P.; Knüsel, P. N.; Antolinez, F. V.; Norris, D. J. High-Temperature Growth of Thick-Shell Cdse/Cds Core/Shell Nanoplatelets. *Chemical Communications.* **2017**, *53*, 9938−9941.
(23) Tessier, M. D.; Spinicelli, P.; Dupont, D.; Patriarche, G.; Ithurria, S.; Dubertret, B. Efficient Exciton Concentrators Built from Colloidal Core/Crown Cdse/Cds Semiconductor Nanoplatelets. *Nano Lett..* **2014**, *14*, 207−213.
(24) Tessier, M. D.; Mahler, B.; Nadal, B.; Heuclin, H.; Pedetti, S.; Dubertret, B. Spectroscopy of Colloidal Semiconductor Core/Shell Nanoplatelets with High Quantum Yield. *Nano Lett..* **2013**, *13*, 3321−3328.
(25) Chen, Z.; Nadal, B.; Mahler, B.; Aubin, H.; Dubertret, B. Quasi-2d Colloidal Semiconductor Nanoplatelets for Narrow Electroluminescence. *Advanced Functional Materials.* **2014**, *24*, 295−302.
(26) Fan, F.; Kanjanaboos, P.; Saravanapavanantham, M.; Beauregard, E.; Ingram, G.; Yassitepe, E.; Adachi, M. M.; Voznyy, O.; Johnston, A. K.; Walters, G.; et al. Colloidal $CdSe_{1-x}S_x$ Nanoplatelets with Narrow and Continuously-Tunable Electroluminescence. *Nano Lett.* **2015**, *15*, 4611−4615.
(27) Guzelturk, B.; Kelestemur, Y.; Olutas, M.; Delikanli, S.; Demir, H. V. Amplified Spontaneous Emission and Lasing in Colloidal Nanoplatelets. *ACS Nano* **2014**, *8*, 6599−6605.
(28) Hamm, P.; Zanni, M.*Concepts and Methods of 2D Infrared Spectroscopy*; Cambridge University Press: New York, 2011.
(29) Sewall, S. L.; Cooney, R. R.; Anderson, K. E. H.; Dias, E. A.; Kambhampati, P. State-to-State Exciton Dynamics in Semiconductor Quantum Dots. *Phys. Rev. B* **2006**, *74*, 235328.
(30) Klimov, V. I. Spectral and Dynamical Properties of Multiexcitons in Semiconductor Nanocrystals. *Annu. Rev. Phys. Chem.* **2007**, *58*, 635−673.
(31) Cooney, R. R.; Sewall, S. L.; Sagar, D. M.; Kambhampati, P. Gain Control in Semiconductor Quantum Dots Via State-Resolved Optical Pumping. *Phys. Rev. Lett.* **2009**, *102*, 127404.
(32) Kambhampati, P. Hot Exciton Relaxation Dynamics in Semiconductor Quantum Dots: Radiationless Transitions on the Nanoscale. *J. Phys. Chem. C* **2011**, *115*, 22089−22109.
(33) Zhang, C.; Do, T. N.; Ong, X.; Chan, Y.; Tan, H.-S. Understanding the Features in the Ultrafast Transient Absorption Spectra of Cdse Quantum Dots. *Chem. Phys.* **2016**, *481*, 157−164.
(34) Do, T. N.; Zhang, C.; Ong, X.; Lian, J.; Chan, Y.; Tan, H.-S. Measuring the Ultrafast Spectral Diffusion Dynamics of Colloidal Cdse Nanomaterials. *MRS Advances.* **2019**, *4*, 1−7.
(35) Palato, S.; Seiler, H.; Nijjar, P.; Prezhdo, O.; Kambhampati, P. Atomic Fluctuations in Electronic Materials Revealed by Dephasing. *Proceedings of the National Academy of Sciences.* **2020**, *117*, 11940−11946.
(36) Caram, J. R.; Zheng, H.; Dahlberg, P. D.; Rolczynski, B. S.; Griffin, G. B.; Dolzhnikov, D. S.; Talapin, D. V.; Engel, G. S. Exploring Size and State Dynamics in Cdse Quantum Dots Using Two-Dimensional Electronic Spectroscopy. *J. Chem. Phys.* **2014**, *140*, 084701.
(37) Seiler, H.; Palato, S.; Sonnichsen, C.; Baker, H.; Kambhampati, P. Seeing Multiexcitons through Sample Inhomogeneity: Band-Edge Biexciton Structure in Cdse Nanocrystals Revealed by Two-Dimensional Electronic Spectroscopy. *Nano Lett..* **2018**, *18*, 2999−3006.
(38) Dong, S.; Lian, J.; Jhon, M. H.; Chan, Y.; Loh, Z. H. Pump-Power Dependence of Coherent Acoustic Phonon Frequencies in

https://doi.org/10.1021/acsnano.2c09606
ACS Nano XXXX, XXX, XXX−XXX

Colloidal Cdse/Cds Core/Shell Nanoplatelets. *Nano Lett.* **2017**, *17*, 3312−3319.
(39) Dong, S.; Pal, S.; Lian, J.; Chan, Y.; Prezhdo, O. V.; Loh, Z. H. Sub-Picosecond Auger-Mediated Hole-Trapping Dynamics in Colloidal Cdse/Cds Core/Shell Nanoplatelets. *ACS Nano* **2016**, *10*, 9370−9378.
(40) Cassette, E.; Pedetti, S.; Mahler, B.; Ithurria, S.; Dubertret, B.; Scholes, G. D. Ultrafast Exciton Dynamics in 2d in-Plane Hetero-Nanostructures: Delocalization and Charge Transfer. *Phys. Chem. Chem. Phys.* **2017**, *19*, 8373−8379.
(41) Akhtar, P.; Do, T. N.; Nowakowski, P. J.; Huerta-Viga, A.; Khyasudeen, M. F.; Lambrev, P. H.; Tan, H. S. Temperature Dependence of the Energy Transfer in Lhcii Studied by Two-Dimensional Electronic Spectroscopy. *J. Phys. Chem. B* **2019**, *123*, 6765−6775.
(42) Dostál, J.; Benesova, B.; Brixner, T. Two-Dimensional Electronic Spectroscopy Can Fully Characterize the Population Transfer in Molecular Systems. *J. Chem. Phys.* **2016**, *145*, 124312.
(43) Do, T. N.; Nguyen, H. L.; Akhtar, P.; Zhong, K.; Jansen, T. L. C.; Knoester, J.; Caffarri, S.; Lambrev, P. H.; Tan, H.-S. Ultrafast Excitation Energy Transfer Dynamics in the Lhcii-Cp29-Cp24 Subdomain of Plant Photosystem Ii. *Journal of Physical Chemistry Letters.* **2022**, *13*, 4263−4271.
(44) Son, M.; Hart, S. M.; Schlau-Cohen, G. S. Investigating Carotenoid Photophysics in Photosynthesis with 2d Electronic Spectroscopy. *Trends in Chemistry.* **2021**, *3*, 733−746.
(45) Nguyen, H. L.; Do, T. N.; Akhtar, P.; Jansen, T. L. C.; Knoester, J.; Wang, W.; Shen, J.-R.; Lambrev, P. H.; Tan, H.-S. An Exciton Dynamics Model of Bryopsis Corticulans Light-Harvesting Complex Ii. *J. Phys. Chem. B* **2021**, *125*, 1134−1143.
(46) Ginsberg, N. S.; Cheng, Y.-C.; Fleming, G. R. Two-Dimensional Electronic Spectroscopy of Molecular Aggregates. *Acc. Chem. Res.* **2009**, *42*, 1352−1363.
(47) Mukamel, S.*Principles of Nonlinear Optical Spectroscopy*; Oxford University Press: New York, 1995.
(48) Do, T. N.; Sim, J. H. N.; Nguyen, H. L.; Lu, Y.; Tan, H. S. Observing the Fluctuation Dynamics of Dative Bonds Using Two-Dimensional Electronic Spectroscopy. *J. Phys. Chem. Lett.* **2021**, *12*, 165−170.
(49) Kwak, K.; Park, S.; Finkelstein, I. J.; Fayer, M. D. Frequency-Frequency Correlation Functions and Apodization in Two-Dimensional Infrared Vibrational Echo Spectroscopy: A New Approach. *J. Chem. Phys.* **2007**, *127*, 124503.
(50) Sanda, F.; Perlik, V.; Lincoln, C. N.; Hauer, J. Center Line Slope Analysis in Two-Dimensional Electronic Spectroscopy. *J. Phys. Chem. A* **2015**, *119*, 10893−10909.
(51) Cichos, F.; Vonborczyskowski, C.; Orrit, M. Power-Law Intermittency of Single Emitters. *Curr. Opin. Colloid Interface Sci.* **2007**, *12*, 272−284.
(52) Pelton, M.; Smith, G.; Scherer, N. F.; Marcus, R. A. Evidence for a Diffusion-Controlled Mechanism for Fluorescence Blinking of Colloidal Quantum Dots. *Proceedings of the National Academy of Sciences.* **2007**, *104*, 14249−14254.
(53) Rabouw, F. T.; van der Bok, J. C.; Spinicelli, P.; Mahler, B.; Nasilowski, M.; Pedetti, S.; Dubertret, B.; Vanmaekelbergh, D. Temporary Charge Carrier Separation Dominates the Photoluminescence Decay Dynamics of Colloidal Cdse Nanoplatelets. *Nano Lett.*. **2016**, *16*, 2047−2053.
(54) Irgen-Gioro, S.; Wu, Y.; López-Arteaga, R.; Padgaonkar, S.; Olding, J. N.; Weiss, E. A. Evidence for Two Time Scale-Specific Blinking Mechanisms in Room-Temperature Single Nanoplatelets. *J. Phys. Chem. C* **2021**, *125*, 13485−13492.
(55) Roberts, S. T.; Loparo, J. J.; Tokmakoff, A. Characterization of Spectral Diffusion from Two-Dimensional Line Shapes. *J. Chem. Phys.* **2006**, *125*, 084502.
(56) Naeem, A.; Masia, F.; Christodoulou, S.; Moreels, I.; Borri, P.; Langbein, W. Giant Exciton Oscillator Strength and Radiatively Limited Dephasing in Two-Dimensional Platelets. *Phys. Rev. B* **2015**, *91*, 121302.
(57) Baghani, E.; O'Leary, S. K.; Fedin, I.; Talapin, D. V.; Pelton, M. Auger-Limited Carrier Recombination and Relaxation in Cdse Colloidal Quantum Wells. *J. Phys. Chem. Lett.* **2015**, *6*, 1032−1036.
(58) Pelton, M.; Ithurria, S.; Schaller, R. D.; Dolzhnikov, D. S.; Talapin, D. V. Carrier Cooling in Colloidal Quantum Wells. *Nano Lett.* **2012**, *12*, 6158−6163.
(59) Sippel, P.; Albrecht, W.; van der Bok, J. C.; Van Dijk-Moes, R. J.; Hannappel, T.; Eichberger, R.; Vanmaekelbergh, D. Femtosecond Cooling of Hot Electrons in Cdse Quantum-Well Platelets. *Nano Lett.* **2015**, *15*, 2409−2416.
(60) Cheng, Y.-C.; Fleming, G. R. Dynamics of Light Harvesting in Photosynthesis. *Annu. Rev. Phys. Chem.* **2009**, *60*, 241−262.
(61) Do, T. N.; Khyasudeen, M. F.; Nowakowski, P. J.; Zhang, Z.; Tan, H. S. Measuring Ultrafast Spectral Diffusion and Correlation Dynamics by Two-Dimensional Electronic Spectroscopy. *Chemistry - An Asian Journal.* **2019**, *14*, 3992−4000.
(62) Le, D. V.; de la Perrelle, J. M.; Do, T. N.; Leng, X.; Tapping, P. C.; Scholes, G. D.; Kee, T. W.; Tan, H.-S. Characterization of the Ultrafast Spectral Diffusion and Vibronic Coherence of Tips-Pentacene Using 2d Electronic Spectroscopy. *J. Chem. Phys.* **2021**, *155*, 014302.
(63) Butkus, V.; Valkunas, L.; Abramavicius, D. Molecular Vibrations-Induced Quantum Beats in Two-Dimensional Electronic Spectroscopy. *J. Chem. Phys.* **2012**, *137*, 044513.
(64) Pal, S.; Nijjar, P.; Frauenheim, T.; Prezhdo, O. V. Atomistic Analysis of Room Temperature Quantum Coherence in Two-Dimensional Cdse Nanostructures. *Nano Lett.*. **2017**, *17*, 2389−2396.
(65) Niehaus, T. A.; Suhai, S.; Della Sala, F.; Lugli, P.; Elstner, M.; Seifert, G.; Frauenheim, T. Tight-Binding Approach to Time-Dependent Density-Functional Response Theory. *Phys. Rev. B* **2001**, *63*, 085108.
(66) Porezag, D.; Frauenheim, T.; Köhler, T.; Seifert, G.; Kaschner, R. Construction of Tight-Binding-Like Potentials on the Basis of Density-Functional Theory: Application to Carbon. *Phys. Rev. B* **1995**, *51*, 12947−12957.
(67) Schoenlein, R. W.; Mittleman, D. M.; Shiang, J. J.; Alivisatos, A. P.; Shank, C. V. Investigation of Femtosecond Electronic Dephasing in Cdse Nanocrystals Using Quantum-Beat-Suppressed Photon Echoes. *Phys. Rev. Lett.* **1993**, *70*, 1014−1017.
(68) Kelley, A. M. Electron-Phonon Coupling in Cdse Nanocrystals from an Atomistic Phonon Model. *ACS Nano* **2011**, *5*, 5254−5262.
(69) Sagar, D. M.; Cooney, R. R.; Sewall, S. L.; Kambhampati, P. State-Resolved Exciton-Phonon Couplings in Cdse Semiconductor Quantum Dots. *J. Phys. Chem. C* **2008**, *112*, 9124−9127.
(70) Lebedev, A. I. Lattice Dynamics of Quasi-Two-Dimensional Cdse Nanoplatelets and Their Raman and Infrared Spectra. *Phys. Rev. B* **2017**, *96*, 184306.
(71) Lebedev, A. I.; Saidzhonov, B. M.; Drozdov, K. A.; Khomich, A. A.; Vasiliev, R. B. Raman and Infrared Studies of Cdse/Cds Core/Shell Nanoplatelets. *J. Phys. Chem. C* **2021**, *125*, 6758−6766.
(72) Tessier, M. D.; Javaux, C.; Maksimovic, I.; Loriette, V.; Dubertret, B. Spectroscopy of Single Cdse Nanoplatelets. *ACS Nano* **2012**, *6*, 6751−6758.
(73) Oron, D.; Aharoni, A.; de Mello Donega, C.; van Rijssel, J.; Meijerink, A.; Banin, U. Universal Role of Discrete Acoustic Phonons in the Low-Temperature Optical Emission of Colloidal Quantum Dots. *Phys. Rev. Lett.* **2009**, *102*, 177402.
(74) Nisoli, M.; De Silvestri, S.; Svelto, O. Generation of High Energy 10 Fs Pulses by a New Pulse Compression Technique. *Appl. Phys. Lett.* **1996**, *68*, 2793−2795.
(75) Hauri, C. P.; Kornelis, W.; Helbing, F. W.; Heinrich, A.; Couairon, A.; Mysyrowicz, A.; Biegert, J.; Keller, U. Generation of Intense, Carrier-Envelope Phase-Locked Few-Cycle Laser Pulses through Filamentation. *Appl. Phys. B: Laser Opt.* **2004**, *79*, 673−677.
(76) Chauhan, V.; Bowlan, P.; Cohen, J.; Trebino, R. Single-Diffraction-Grating and Grism Pulse Compressors. *J. Opt. Soc. Am. B* **2010**, *27*, 619.

https://doi.org/10.1021/acsnano.2c09606
ACS Nano XXXX, XXX, XXX−XXX

(77) Zhang, Z.; Wells, K. L.; Hyland, E. W. J.; Tan, H.-S. Phase-Cycling Schemes for Pump-Probe Beam Geometry Two-Dimensional Electronic Spectroscopy. *Chem. Phys. Lett.* **2012**, *550*, 156−161.

https://doi.org/10.1021/acsnano.2c09606
ACS Nano XXXX, XXX, XXX−XXX